

## Accepted Manuscript

Biochemical and thermodynamic comparison of the selenocysteine containing and non-containing thioredoxin glutathione reductase of *Fasciola gigantica*

Parismita Kalita, Harish Shukla, Rohit Shukla, Timir Tripathi

PII: S0304-4165(18)30063-1  
DOI: [doi:10.1016/j.bbagen.2018.03.007](https://doi.org/10.1016/j.bbagen.2018.03.007)  
Reference: BBAGEN 29058

To appear in:

Received date: 14 November 2017  
Revised date: 2 March 2018  
Accepted date: 6 March 2018

Please cite this article as: Parismita Kalita, Harish Shukla, Rohit Shukla, Timir Tripathi, Biochemical and thermodynamic comparison of the selenocysteine containing and non-containing thioredoxin glutathione reductase of *Fasciola gigantica*. The address for the corresponding author was captured as affiliation for all authors. Please check if appropriate. *Bbagen*(2018), doi:[10.1016/j.bbagen.2018.03.007](https://doi.org/10.1016/j.bbagen.2018.03.007)

This is a PDF file of an unedited manuscript that has been accepted for publication. As a service to our customers we are providing this early version of the manuscript. The manuscript will undergo copyediting, typesetting, and review of the resulting proof before it is published in its final form. Please note that during the production process errors may be discovered which could affect the content, and all legal disclaimers that apply to the journal pertain.



**Biochemical and thermodynamic comparison of the selenocysteine containing and non-containing thioredoxin glutathione reductase of *Fasciola gigantica***

Parismita Kalita, Harish Shukla, Rohit Shukla, and Timir Tripathi\*

Molecular and Structural Biophysics Laboratory, Department of Biochemistry, North-Eastern Hill University, Shillong 793022, India

*Running title: Comparison of FgTGRsec and FgTGR*

\*To whom correspondence should be addressed: Dr. Timir Tripathi, Department of Biochemistry, North-Eastern Hill University, Shillong- 793022, India. Email: timir.tripathi@gmail.com, ttripathi@nehu.ac.in. Tel: +91-364-2722141; Fax: +91-364-2550108.

**ABSTRACT**

The thiol-disulfide redox metabolism in platyhelminth parasites depends entirely on a single selenocysteine (Sec) containing flavoenzyme, thioredoxin glutathione reductase (TGR) that links the classical thioredoxin (Trx) and glutathione (GSH) systems. In the present study, we investigated the catalytic and structural properties of different variants of *Fasciola gigantica* TGR to understand the role of Sec. The recombinant full-length Sec containing TGR (FgTGRsec), TGR without Sec (FgTGR) and TGRsec without the N-terminal glutaredoxin (Grx) domain ( $\Delta$ NTD-FgTGRsec) were purified to homogeneity. Biochemical studies revealed that Sec597 is responsible for higher thioredoxin reductase (TrxR) and glutathione reductase (GR) activity of FgTGRsec. The N-terminal Grx domain was found to positively regulate the DTNB-based TrxR activity of FgTGRsec. The FgTGRsec was highly sensitive to inhibition by auranofin (AF). The structure of FgTGR was modeled, and the inhibitor AF was docked, and binding sites were identified. Unfolding studies suggest that all three proteins are highly cooperative molecules since during GdnHCl-induced denaturation, a monophasic unfolding of the proteins without stabilization of any intermediate is observed. The  $C_m$  for GdnHCl induced unfolding of FgTGR was higher than FgTGRsec and  $\Delta$ NTD-FgTGRsec suggesting that FgTGR without Sec was more stable in solution than the other protein variants. The free energy of

stabilization for the proteins was also determined. To our knowledge, this is also the first report on unfolding and stability analysis of any TGR.

## Keywords

Platyhelminthes, parasite, liver fluke, thioredoxin glutathione reductase, glutathione reductase, thioredoxin reductase, glutathione, activity, homology modeling, auranofin, inhibition

## 1. INTRODUCTION

Enzymes associated with redox metabolism encompass the most interesting targets for drug development against infectious diseases. These enzymes maintain cellular homeostasis and play a major role in antioxidant defenses [1]. A disturbed redox metabolism results in the alteration of several important cellular processes that are critical for proper cell function. The redox regulation is mainly accomplished by oxidative modification of the highly susceptible thiol group (-SH) of the cysteinyl side chain of proteins [2]. Hence, being crucial players in redox regulation, the thiol-proteins become the most vulnerable targets of cellular redox imbalance.

All organisms are equipped with a variety of antioxidant thiol-based enzymes that maintain the cellular redox homeostasis. In most aerobic organisms it is comprised of two separate redox systems: the glutathione/glutaredoxin (GSH/Grx) system containing Grx, GSH and NADPH-dependent glutathione reductase (GR); and the thioredoxin (Trx) system containing Trx and NADPH-dependent thioredoxin reductase (TrxR) [3]. In contrast to these classical redox systems, the platyhelminth parasites contain a single multifunctional selenocysteine (Sec, U) containing flavoenzyme, thioredoxin glutathione reductase (TGR), having fused Grx and TrxR domains that link both these systems [4, 5]. Transcriptomic and genomic data of *F. hepatica*, *T. solium*, *Schistosoma sp.* and *E. multicularis* reveals the absence of GR and TrxR genes in these parasites [6, 7]. TGR is the sole enzyme responsible for both Trx and GSH reduction in parasitic flukes. In the absence of catalase, the cellular redox homeostasis of these parasites depends entirely on the TGR, which supplies electrons to both glutathione disulfide (GSSG) and Trx. Also, TGR is the key enzyme responsible for reactive oxygen species (ROS) detoxification, redox homeostasis maintenance, and synthesis of deoxyribonucleotides in parasitic flukes [8, 9]. Helminth TGR encodes a Sec in its C-terminal end. Sec is the 21<sup>st</sup> amino acid encoded by the UGA codon in the mRNA and it acts as an important active site residue in many redox active

selenoenzymes such as TGR, TrxR, glutathione peroxidase (GPx), iodothyronine deiodinase, etc, in all forms of life [10, 11]. Its role is also implicated in redox signaling, antioxidant defense, thyroid hormone metabolism and immune response [11]. Co-translational incorporation of Sec into the polypeptide chain involves a complex machinery that includes a SECIS element (selenocysteine insertion sequence), SECIS binding protein (SBP1 and SBP2), a Sec-tRNA<sup>[Ser]Sec</sup>, Sec specific elongation factor and other accessory proteins[10]. Several structures of TGR have been determined [7, 12, 13]. The X-ray crystallographic structure of *S. mansoni* TGR shows that like other members of the pyridine nucleotide disulfide oxidoreductase family, it is a homodimeric protein with monomers arranged in a head-to-tail fashion creating a twisted 'W' shape [14]. Each monomer is composed of two key domains: an N-terminal Grx domain and a C-terminal TrxR domain. The two Grx domains are at the top of the two outer arms of the dimer 'W'. In addition to an NADPH binding site, the TrxR domain has two redox active centers viz. a -CX<sub>4</sub>C- motif in the FAD-binding domain (also found in GR and TrxR) and a Sec containing -GCUG- redox center in the C-terminus. The Grx domain has a GSH binding site and a redox active Cys pair (-CXXC- or -CXXS-) [15]. The dithiol Grx containing TGR exhibits a unique hysteresis phenomenon as its GR activity is regulated by the [GSSG]/[GSH] ratio. Under high GSSG concentrations, the GR activity of TGR decreases and the behavior is reverted in the presence of GSH, Trx, or DTT. This behavior is associated with glutathionylation of TGR by GSSG and is blocked by deglutathionylation [16, 17]. In contrast, the monothiol Grx containing TGR shows no hysteresis for GR activity [18].

Fascioliasis is a major food borne tropical disease caused by the organisms of the genus *Fasciola*. It affects over 600 million animals globally resulting in economic losses of >US\$3 billion p.a. in livestock production. Around 25–100% of cattle in Africa, the Middle East, and Southeast Asia are affected annually and in temperate countries it also affects ~70% of humans [19]. It is estimated that around 2.4–17 million people are infected and approximately 180 million people are at risk globally [20]. Africa, Europe, the Middle East (including Egypt), Southeast Asia, and Latin America, are listed as the major human fascioliasis endemic areas, with Bolivian Altiplano having the highest prevalence [21, 22]. Triclabendazole (TCZ) is the only drug of choice recommended by WHO against these flukes [23]. Recent reports of TCZ resistance highlight the need for new chemotherapeutics [24–28]. With the help of antioxidant enzymes, these parasites can scavenge the reactive species produced as a result of host immune

response and can survive in the host for longer periods. In recent years, TGR has emerged as a rational drug target for the treatment of platyhelminthic infections as it is not present in the human counterparts. Auranofin, an inhibitor of TGR and TrxRs, kills larval worms *in vitro* and has been reported to partially cure *Schistosoma* infection [29, 30]. Besides auranofin, several other inhibitors have also been identified for TGRs [31-35]. Limited knowledge is available regarding the structure-function relationship of redox enzymes of parasitic flukes. In the present study, we have investigated the structure-function relationship, stability and folding analysis of FgTGRsec and its truncated variants to define the molecular, functional and structural characteristics of this enzyme.

## **2. MATERIALS AND METHODS**

### **2.1 Materials**

The molecular biology kits and Ni-NTA agarose were purchased from Qiagen, CA, USA. The dNTPs and enzymes were purchased from New England Biolabs, MA, USA. All other reagents and chemicals were purchased either from Sigma-Aldrich Chemical Company, St. Louis, MO, USA, or Sisco Research Laboratories, Mumbai, India and were of the highest purity available. Bacterial culture media was purchased from Himedia Laboratories, Mumbai, India.

### **2.2 Collection and identification of parasites**

The adult liver flukes were collected from the liver of naturally infected cattle from the local slaughterhouse at Bada Bazaar, Shillong, India. The flukes were washed extensively with chilled phosphate buffer saline (pH 7.5). The flukes were identified as *F. gigantica* using morphological properties.

### **2.3 Isolation of total RNA and cDNA synthesis**

The flukes were crushed in a pestle and mortar with liquid nitrogen, and the total RNA was isolated using the RNeasy mini kit (Qiagen, USA) as per the manufacturer instructions. The first strand cDNA was synthesized using QuantiTect Reverse Transcriptase kit (Qiagen, USA) as per the manufacturer instructions.

### **2.4 Cloning, overexpression and purification of FgTGRsec and $\Delta$ NTD-FgTGRsec**

*Fgtgrsec* and  $\Delta$ NTD-*Fgtgrsec* were amplified by PCR using primers containing a bacterial type SECIS element for Sec insertion. Three sets of primers were designed based on the full length TGR sequence of *F. gigantea* (Supplementary Table 1). The reverse primer of both FgTGRsec and  $\Delta$ NTD-FgTGRsec contained a bacterial type SECIS for Sec insertion, whereas that of FgTGR was designed without a bacterial-type SECIS. The stop codon of the gene was omitted in the reverse primers and the resulting peptide ends at stop codon coded by the SECIS element. The amplicons were cloned into pSK+ vector and further sub-cloned to pET23a(+) (Amp<sup>+</sup>) and pET28a(+) (Kan<sup>+</sup>) vectors, respectively. The method described by Kuntz et al. was followed for expression of the recombinant selenoproteins [7]. The recombinant plasmids were transformed into competent *E. coli* BL21 (DE3) expression host cells and grown in Luria-Bertani media containing respective antibiotics at 37 °C until an  $A_{600} \sim 0.7$  was achieved and then induced at 20 °C with 0.5 mM Isopropyl  $\beta$ -D-1-thiogalactopyranoside (IPTG). Also, as a source of selenium, 5  $\mu$ M Na<sub>2</sub>SeO<sub>3</sub> was added to the induced culture and 10% glycerol was added for enhancing solubility and to ensure slow growth. Induced cultures were further grown for ~12 h with continuous shaking at 150 rpm and 20 °C. After sonication, the clear cell lysate was loaded onto a Ni-NTA column pre equilibrated with 50 mM phosphate buffer (pH 8.0), containing 300 mM NaCl and washed with the same buffer to remove unbound contaminants. The column was washed with increasing concentrations of imidazole, and the proteins were eluted with equilibration buffer containing 300 mM imidazole. The purified proteins were dialyzed against 20 mM phosphate buffer (pH 8.0), containing 150 mM NaCl. Overexpression and purification of truncated FgTGR were performed as mentioned earlier [36]. The purity and the molecular weight of the recombinant protein were determined using 12% SDS-PAGE. Quantitation of the recombinant proteins was carried out using the Bradford method using bovine serum albumin as the standard.

## 2.5 Size exclusion chromatography (SEC)

SEC experiments were carried out on a Superdex™ 200 10/300 GL column on an AKTA FPLC (GE Healthcare Biosciences, USA) pre-calibrated with standard molecular weight markers. The column was equilibrated and run with 20 mM phosphate buffer (pH 8.0), containing 150 mM NaCl at 25 °C at a flow rate of 0.4 mL/min with detection at 280 nm and 450 nm for detection of protein and bound FAD respectively.

## 2.6 Biochemical assays

TrxR and GR activities of FgTGRsec, FgTGR and  $\Delta$ NTD-FgTGRsec were analyzed in a Cary 50 (Varian) spectrophotometer at 25 °C based on the methods described by Kuntz *et al.*[7]. The TrxR activity was determined by the 5,5'-dithiobis(2-nitrobenzoic acid) (DTNB) reduction assay. The assay solution contained 1  $\mu$ M recombinant enzyme, 200  $\mu$ M NADPH and 10 mM EDTA in 20 mM phosphate buffer (pH 7.2), containing 150 mM NaCl. The DTNB concentration was varied from 0.5 mM to 5 mM. The increase in absorbance at 412 nm during the first three min was monitored, and the extinction coefficient of 13.6  $\text{mM}^{-1}\text{cm}^{-1}$  for 5-thionitrobenzoic acid (TNB) was used for calculation of activity.

The GR activity was determined using GSSG. The reaction mixture contained 1  $\mu$ M recombinant enzyme, 200  $\mu$ M NADPH and 1 mM EDTA in 20 mM phosphate buffer (pH 7.2) and 150 mM NaCl. The GSSG concentration was varied from 0.5  $\mu$ M to 5  $\mu$ M. The decrease in NADPH consumption at 340 nm during the first three min was monitored, and the extinction coefficient of 6.22  $\text{mM}^{-1}\text{cm}^{-1}$  for NADPH was used for calculation of activity.

## 2.7 Inhibition studies

To assess the effect of the inhibitor auranofin (AF) on FgTGRsec, incubation mixtures were prepared containing 3  $\mu$ M FgTGRsec with and without AF (0.5 to 5  $\mu$ M). For DTNB-based TrxR activity inhibition assay, reaction mixtures were prepared as mentioned above. The measurements were performed at 120 min after incubation. The reaction was initiated by addition of 5 mM DTNB and followed by the increase in absorbance at 412 nm.

For GR activity inhibition assay, reaction mixtures were prepared as mentioned above. The measurements were performed at 120 min after incubation. The reaction was initiated by addition of 500  $\mu$ M GSSG and followed by the decrease in absorbance at 340 nm.

## 2.8 Fluorescence quenching with substrates and inhibitor

For fluorescence quenching experiments, the stock solutions of the quenchers - DTNB (5 mM), GSSG (10 mM) and AF (250  $\mu$ M) were prepared separately. Each quencher was added to achieve the desired range of quencher concentration in 1  $\mu$ M protein sample. The samples were excited at 280 nm and the emission spectra were recorded in the range of 300–500 nm. The

Stern-Volmer quenching constants were calculated using the plot of  $F_0/F_1$  values against the input concentration of quenchers, in the Stern-Volmer equation,

$$F_0/F_1 = 1 + K_{SV} [Q]$$

where  $F_0$  and  $F$  are the fluorescence intensities at a particular wavelength in the absence and presence of quencher, respectively,  $K_{sv}$  is the Stern-Volmer constant, and  $[Q]$  is the concentration of the quencher.

## 2.9 Equilibrium unfolding experiments

A stock solution of 8 M GdnHCl was prepared in 20 mM phosphate buffer (pH 7.2) containing 150 mM NaCl. All samples were incubated for 4 h to achieve denaturation equilibrium before the readings were taken.

## 2.10 Fluorescence and circular dichroism (CD) spectroscopy

Fluorescence spectra were recorded with Perkin-Elmer Life Sciences LS55 fluorescence spectrometer in a 10 mm path length quartz cuvette. Protein concentration used was 1  $\mu$ M for all experiments and the measurements were carried out at 25 °C. Slit width for both emission and excitation were kept as 10 nm. For monitoring Trp and FAD fluorescence, the excitation wavelength of 285 nm and 445 nm, respectively, were used and the spectra were recorded between 300-500 nm and 450-600 nm, respectively.

The CD measurements were made on JASCO J1500 spectropolarimeter calibrated with ammonium ( $\beta$ )-10-camphorsulfonate with a 5 mm path length cell at 25 °C at a protein concentration of 1  $\mu$ M. Three consecutive scans were accumulated and an average spectra was stored. The values obtained were normalized by subtracting the baseline recorded for the buffer under similar conditions.

## 2.11 Calculation of free energy of stabilization

Following a two-state model of unfolding of a protein, the CD and fluorescence spectroscopic data were converted into the free energy of unfolding for each data point ( $\Delta G_D$ ). The  $\Delta G_D$  values were then plotted against [GdnHCl] to determine the free energy of stabilization in the absence of denaturants ( $\Delta G_D^{H_2O}$ ) according to the linear extrapolation method [37] as described earlier [38-41].

### 2.12 Homology modeling and validation

Homology modeling was performed using Modeller 9.16 [42]. Initially, the BLAST (<http://blast.ncbi.nlm.nih.gov/Blast.cgi>) search was performed to find the closely related homologs of FgTGRsec and then template was selected on the basis of identity, query coverage and structure resolution. The structure of *S. japonicum* TGR (SjTGR) (PDB ID: 4LA1) [12] was taken as the template to model the dimeric FgTGRsec. The obtained structure was superimposed with the model to find the reliability using Chimera 1.10.2 [43]. Modeled structure was validated using ProSA [44], PROCHECK [45] and Verify 3D server [46]. The secondary structure was predicted by using SOPMA tool.

### 2.13 Molecular docking

Molecular docking of FgTGRsec with AF was performed by using Molegro Virtual Docker (MVD) as earlier [47, 48]. The structure of AF and TP gold moiety were drawn using Chemdraw followed by energy minimization of ligand structures by Amberff99SB force field using Chimera 1.10.2. Prior to docking, the protein structure was prepared using MVD [49]. The best pose having the energetically favorable structure was selected. MVD calculated the interaction energies between ligands and protein. The MolDock Score was used for energy calculation. The residues defined in previous studies were selected for molecular docking [31]. The cavity used for virtual screening had the size constraint of 15 Å. The docking parameters for virtual screening included the number of runs (100), population size (50), max iterations (2,000), scaling factor (0.50), and crossover rate (0.90). Ten binding pose were generated by molecular docking and selected on the basis of binding affinity as well as best binding conformation.

## 3. RESULTS

### 3.1 Purification of FgTGRsec, FgTGR and $\Delta$ NTD-FgTGRsec

The full-length Sec containing TGR (FgTGRsec), TGR without Sec and the last amino acid (FgTGR) and TGR without the N-terminal Grx domain ( $\Delta$ NTD-FgTGRsec) were purified as described above. The purified proteins were homogenous as indicated by single protein bands of ~66 kDa for both FgTGRsec and FgTGR; and ~54 kDa for  $\Delta$ NTD-FgTGRsec, respectively on SDS-PAGE (Fig. 1A). The molecular mass of purified recombinant FgTGRsec, FgTGR and

$\Delta$ NTD-FgTGRsec were determined under non-dissociating conditions by size-exclusion chromatography (SEC). Gel filtration of the recombinant proteins on Superdex<sup>TM</sup> S-200 column calibrated with various molecular weight standards showed a single peak for each protein at 280 nm with retention volumes of 13.70 mL, 13.65 mL and 14.15 mL, respectively (Fig. 1B). The deep yellow color of the proteins indicated the presence of bound FAD that was confirmed through the 450 nm absorbance peaks for all proteins in SEC (data not shown). When the elution volumes of the marker proteins were plotted as a function of log of molecular weight, the FgTGRsec, FgTGR and  $\Delta$ NTD-FgTGRsec were found to have molecular weights of about 132 kDa, 132 kDa and 108 kDa, respectively.

### 3.2 Structural characteristics of the recombinant proteins

The Trp fluorescence spectra of FgTGRsec, FgTGR and  $\Delta$ NTD-FgTGRsec are shown in Figure 2A. An emission wavelength of about 336 nm, 334 nm and 340 nm was observed for the recombinant FgTGRsec, FgTGR and  $\Delta$ NTD-FgTGRsec, respectively. The sequences of FgTGRsec, FgTGR and  $\Delta$ NTD-FgTGRsec encode 9, 9 and 8 Trp residues, respectively. In general, the buried Trp residues in folded protein show fluorescence emission maxima between 330-335 nm [50, 51]. Thus the Trp residues in FgTGRsec and FgTGR are predominantly buried in the hydrophobic core. The analysis of far-UV CD spectra demonstrates the presence of  $\alpha/\beta$  type secondary structure (Fig. 2B) in all the three proteins. From these results, it is evident that all these proteins are present in the properly folded conformation.

### 3.3 Sec597 is responsible for higher DTNB-based TrxR activity in FgTGRsec

Recombinant FgTGRsec encodes a Sec at position 597. A decrease in fluorescence intensity was observed following the binding of DTNB with FgTGRsec and FgTGR (Supplementary Fig. 1). The extent of quenching was greater in the case of FgTGRsec (~300% decrease from the starting point) than the FgTGR (~ 200% decrease from the start). The comparative larger reduction in the intrinsic fluorescence of FgTGRsec observed upon DTNB binding with respect to FgTGR suggests that FgTGRsec may have a greater affinity for DTNB than FgTGR. The fluorescence data were further analyzed using the Stern–Volmer plot. Higher  $K_{sv}$  of FgTGRsec ( $60.6 \times 10^{-3} \mu\text{M}^{-1}$ ) confirmed the higher affinity of DTNB towards FgTGRsec than FgTGR ( $42.5 \times 10^{-3} \mu\text{M}^{-1}$ ) (Fig. 3A and Table 1).

We then performed comparative enzymatic activity analysis of FgTGRsec and FgTGR with DTNB. It was observed that FgTGRsec showed higher activity than FgTGR (Fig. 3B). The result of activity analysis is in corroboration with the binding profile of DTNB with FgTGRsec and FgTGR. The decrease in activity of FgTGR may be attributed to the absence of Sec at the C-terminal region of the protein that is necessary to attain optimal catalytic behavior.

### 3.4 FgTGRsec has higher GR activity with respect to FgTGR

The N-terminal Grx domain of TGR is also involved in the GR activity. Studies suggest that there are two different binding sites for GSSG, one at the Grx domain and another in the TrxR domain. Also, some TGR truncations lacking Grx domain were found incapable of reducing GSSG [52-54].  $\Delta$ NTD-FgTGRsec also showed almost no/negligible GR activity in absence of Grx domain (data not shown). Moreover, Grx domain contacts with the N-terminal part of the TrxR domain, thus allowing a shorter route of the electron transfer [55]. To characterize this activity, GSSG was used as a substrate. For comparative analysis of the binding of GSSG with FgTGRsec and FgTGR, fluorescence quenching analysis was performed. A decrease in the quantum yield of fluorescence with increasing concentration of GSSG represents the binding of GSSG with the protein. The fractional change in quenching was found to be greater for FgTGRsec than FgTGR (Supplementary Fig. 2). Stern-Volmer analysis of quenching experiment suggested that the binding affinity of GSSG with FgTGRsec ( $K_{sv} = 0.7 \times 10^{-3} \mu\text{M}^{-1}$ ) is greater than that of FgTGR ( $K_{sv} = 0.5 \times 10^{-3} \mu\text{M}^{-1}$ ) (Fig. 3C and Table 1). This implies that FgTGRsec may have higher GR activity than FgTGR due to favorable GSSG binding. To confirm this, we performed the GR activity analysis of FgTGRsec and FgTGR with GSSG and observed that FgTGRsec indeed shows higher GR activity than FgTGR (Fig. 3D and Table 2).

### 3.5 The N-terminal Grx domain positively regulates the DTNB-based TrxR activity of FgTGRsec

To examine the possible role of the N-terminal Grx domain in the DTNB-based TrxR activity of FgTGRsec, we constructed a truncation for FgTGRsec lacking the N-terminal Grx domain (residues 1 to 109) ( $\Delta$ NTD-FgTGRsec). The structural feature of the  $\Delta$ NTD-FgTGRsec has been discussed in section 2.2. To analyze the effect of Grx domain on the DTNB-based TrxR activity of the proteins, we performed two sets of experiments. Firstly, we determined the comparative

binding analysis of DTNB with FgTGRsec and  $\Delta$ NTD-FgTGRsec using fluorescence quenching. Stern-Volmer analysis of quenching experiment suggested that the binding affinity of DTNB to  $\Delta$ NTD-FgTGRsec ( $K_{sv} = 52.2 \times 10^{-3} \mu\text{M}^{-1}$ ) was slightly less than that of full length FgTGRsec ( $K_{sv} = 60.6 \times 10^{-3} \mu\text{M}^{-1}$ ) (Fig. 4A and Table 1). The extent of quenching was greater in FgTGRsec than  $\Delta$ NTD-FgTGRsec (Supplementary Fig. 3), which suggests that the binding of DTNB was partly compromised in the  $\Delta$ NTD-FgTGRsec. To confirm whether this binding pattern correlates with the activity, we performed activity assay and found that  $\Delta$ NTD-FgTGRsec exhibited about two-fold lesser DTNB-based TrxR activity when compared with the FgTGRsec (Fig. 4B and Table 2). These results suggest that the N-terminal Grx domain has a positive role in regulating TrxR activity.

### 3.6 Binding and inhibition of catalytic activity of FgTGRsec by AF

AF is a gold-containing compound that binds to and inhibits TGRsec activity of several parasitic flukes [13, 17, 30, 56, 57]. To evaluate the effect of AF on the activity of FgTGRsec, inhibition studies were performed. Stern-Volmer analysis of quenching experiment shows strong binding affinity of AF with FgTGRsec ( $K_{sv} = 58.8 \times 10^{-3} \mu\text{M}^{-1}$ ) (Supplementary Fig. 4) (Fig. 5A). AF inactivates the activity of FgTGRsec in a concentration dependent manner (Fig. 5B) with an  $IC_{50}$  of 0.87  $\mu\text{M}$  for DTNB-based TrxR activity and 8.30  $\mu\text{M}$  for GR activity (Fig.5C). Both TrxR and GR activities were found to be decreased by  $\sim 10$  fold at  $\sim 2 \mu\text{M}$  concentration of AF at a fixed concentration of DTNB and GSSG, respectively.

### 3.7 Homology modeling, energy minimization and structure validation of FgTGR

The crystal structure of FgTGRsec is not available so we modelled the structure of FgTGR. The sequence was submitted to PDB BLAST for predicting homolog structures. The crystal structure of SjtGR (PDB ID: 4LA1) was selected as a template for modeling the FgTGR structure. We found 99% query coverage with 63% sequence identity in pairwise sequence alignment. The predicted structure was modified with the Sec residue. The structure alignment between SjtGR and FgTGRsec was carried out to predict the reliability of the modelled structure. The RMSD value was found to be 0.277  $\text{\AA}$  which indicates that the predicted model is very close and similar to the template structure. The sequence alignment and structure alignment of FgTGRsec with SjtGR is shown in supplementary Figure 5 and 6. The structure was further validated by using

Ramachandran plot, Z score and Verify-3D score. Ramachandran plot showed that most of the amino acids were present in most favored region with 5.8% in additional allowed region and only three residues (263, 519 and 521) belong to the disallowed region (Supplementary Fig. 7). The energy window of FgTGRsec model showed that only some of the C-terminal residues lie in the positive window while all other residues belong to the negative window (Supplementary Fig. 8) indicating that the overall energy of the model is good. The Z-score of the predicted model (-12.25) was similar to the template structure (-12.41) suggesting that the accuracy of predicted model is good (Supplementary Fig. 9). The verify-3D showed a score of 95.48% for FgTGRsec that suggests the good quality of the model (Supplementary Fig. 10). All the stereo-chemical parameters suggested that the predicted model was good and can be used for further analysis. The stereochemical parameters of FgTGRsec were found to be the same as our previous study with FgTGR model [31]. The SOPMA server was used to predict the secondary structure content of FgTGRsec. The percentage of  $\alpha$ -helix, extended strand,  $\beta$ -turn and random coil were found to be 31.44%, 25.08%, 10.70% and 32.78% respectively.

### 3.8 Molecular docking

AF was docked against FgTGRsec to predict the binding pattern. It showed binding with several catalytic residues with a good docking score. AF showed -141.32 MolDock Score with five hydrogen bonds. The Sec597 from chain A and Lys125, Gln216 from chain B were involved in hydrogen bonding with FgTGRsec. Sec597 form a hydrogen bond between the N-atom of the AF and its own amide group. The amide group of catalytically important polar amino acid Lys125 interacts with the O-atom of the ligand by hydrogen bond. Gln216 form three hydrogen bonds with the ligand. The amide group of the polar amino acid Gln216 interacts with the three O-atom of the ligand. The residues Ala595, Thr594, Sec597, Thr580, Ser504, Glu576 and Val593 from chain A and Leu209, Tyr213, Gln216, Lys125, Arg451, Ile447 from chain B are involved in hydrophobic interactions (Fig. 6A). AF interacts with both the chains and also with the catalytically important amino acid residues.

### 3.9 Triethylphosphine-gold moiety (TP gold)

A crystal structure of TGR in complex with gold has been reported by Angelucci et.al [56]. In this structure, they co-crystallized AF with SmTGR and predicted the binding of gold to the

protein. They found that gold binds at three places. We also docked a single TP gold moiety to FgTGRsec to predict its binding pattern. We found that it shows a MolDock Score of -52.57 that is less than AF. This is due to the larger size of AF that leads to higher binding affinity. The TP gold moiety did not form any hydrogen bond with the protein though it showed hydrophobic interactions with residues- Phe506, Pro508, Leu509, His571, Pro572, Glu576 and Cys574. Interestingly, during the gold binding, the position of the gold moiety was changed, and it showed very close interaction with a catalytically important amino acid His571 with a distance of 3.847 Å (Fig. 6B).

### **3.10 GdnHCl-induced changes in structural and functional properties of FgTGRsec and FgTGR**

To study the difference in the folding behavior and conformational stability of FgTGRsec and FgTGR, GdnHCl-induced unfolding of both the proteins was studied. Figure 7A summarizes the changes in Trp emission maxima of both FgTGRsec and FgTGR with increasing concentrations of GdnHCl. A sigmoidal loss in the emission maxima of FgTGRsec and FgTGR from 336 nm and 334 nm, respectively to about 356 nm was observed between 0 and 4 M GdnHCl. At GdnHCl above 4.0 M, the emission maxima reached 356 nm demonstrating that the proteins are completely unfolded under these conditions as the exposed Trp residues in an unfolded protein show emission maximum between 350-356 nm [51]. To test whether the two-state unfolding of FgTGRsec and FgTGR reflects the disruption of the overall structure of the proteins or is merely an indicative of local unfolding near the Trp microenvironment, we studied the GdnHCl-induced alterations in the secondary structure of the proteins. Figure 7A also summarizes the effect of increasing concentrations of GdnHCl on the CD ellipticity at 222 nm for FgTGRsec and FgTGR. Increase in GdnHCl concentrations between 0.5 and 3.0 M GdnHCl resulted in a gradual decrease in CD ellipticity at 222 nm of FgTGRsec, and almost complete loss of CD signal was observed at about 3.5 M GdnHCl. For FgTGR complete loss of CD signal was observed at about 4.0 M GdnHCl. Thus, the far-UV CD results show that FgTGRsec unfolded at a lower GdnHCl concentration than FgTGR, which was similar to that observed from changes in tryptophan fluorescence. The average  $C_m$  calculated from fluorescence and CD signal of FgTGRsec was found to be ~2.1 M while that of FgTGR was observed at ~2.4 M (Table 2).

FgTGRsec contains a single, tightly but non-covalently bound FAD molecule and nine Trp residues in each subunit. In the structure of FgTGRsec, the FAD moiety is present towards the interior of the protein core. It is well known that a strong correlation between alterations in enzymatic activity and FAD fluorescence polarization exists in flavoproteins. Hence, we monitored the changes in FAD fluorescence polarization of FgTGRsec and FgTGR at increasing GdnHCl concentrations. A sharp decrease in the fluorescence polarization and the GR activity of FgTGRsec and FgTGR was observed between 0 and 1 M GdnHCl and beyond this concentration a complete loss of activity was observed (Fig. 7B). This suggests a slight perturbation in the Grx domain active site that is involved in GR activity of the protein. The DTNB-based TrxR activity also showed gradual decrease between 0 and 2 M GdnHCl. Beyond this denaturant concentration a complete loss of polarization as well as activity occurs. Interestingly, both FgTGRsec and FgTGR showed an initial increase in the DTNB-based TrxR activity at 0.25 M and 0.5 M GdnHCl concentration that may be due to slight melting of the secondary structure making the active site more accessible to substrate (DTNB) binding. At these concentrations, even though FgTGR showed ~2 fold higher activity than the FgTGRsec, its activity decreased abruptly beyond 1.0 M GdnHCl while complete loss of DTNB-based TrxR activity of FgTGRsec was seen beyond 2.5 M (Fig.7C).

We further determined the conformational stability of FgTGRsec and FgTGR assuming the two-states model of unfolding. The GdnHCl-induced unfolding curves of both fluorescence and far-UV CD experiments were used to determine the free energy of stabilization in the absence of denaturants ( $\Delta G_D^{H2O}$ ) by linear extrapolation of the  $\Delta G_D$  values to zero denaturant concentration (Fig. 7D). From these measurements, a comparable  $\Delta G_D^{H2O}$  value for FgTGRsec was calculated to be around 16.32 kcal.mol<sup>-1</sup> and 16.24 kcal.mol<sup>-1</sup>, respectively. Similarly, the  $\Delta G_D^{H2O}$  value for FgTGR was calculated to be around 17.96 kcal.mol<sup>-1</sup> and 17.35 kcal.mol<sup>-1</sup>, respectively.

### 3.11 Comparison of GdnHCl-induced changes in structural and functional properties of FgTGRsec and $\Delta$ NTD-FgTGRsec

To understand the effect of the N-terminal Grx domain in the unfolding of TGR, GdnHCl induced unfolding of FgTGRsec and  $\Delta$ NTD-FgTGRsec was studied. GdnHCl induced unfolding of  $\Delta$ NTD-FgTGRsec also showed cooperative transitions in both fluorescence and far-UV CD

spectroscopy (Fig. 8A). These results showed a sigmoidal loss of structure in both proteins leading to the complete loss in structure beyond 3.5 M GdnHCl. The correlation between FAD polarization and its DTNB-based TrxR activity was also monitored for  $\Delta$ NTD-FgTGRsec. A significant decrease in FAD polarization and activity was observed between 0 and 1.0 M GdnHCl concentration (Fig. 8B). Similar to that of the full-length FgTGRsec,  $\Delta$ NTD-FgTGRsec also showed an initial increase in its activity between 0.25 to 0.5 M GdnHCl, but beyond 1.0 M GdnHCl, complete loss of activity was observed. Also, a lower  $C_m$  value of  $\Delta$ NTD-FgTGRsec (~1.9 M) suggests that it is comparatively less stable than the FgTGRsec (~2.1 M) (Table 2).

From these measurements, a comparable  $\Delta G_D^{H2O}$  value for  $\Delta$ NTD-FgTGRsec was calculated to be around 15.98 kcal.mol<sup>-1</sup> and 15.90 kcal.mol<sup>-1</sup>, respectively, which is slightly less than that of the full-length FgTGRsec, suggesting a relatively feasible thermodynamic process for  $\Delta$ NTD-FgTGRsec unfolding by GdnHCl (Fig. 8C).

#### 4. DISCUSSION

The redox homeostasis of parasites is precarious due to the oxidative stress imposed by the host, and in the case of parasitic helminths, it is absolutely dependent on selenium. This has led to successful targeting of TGR in these parasites. Parasitic flukes have a unique and simplified thiol-based redox system. It represents an unusual fusion of the conventional Trx and GSH system, where a single enzyme TGR supplies electrons to both Trx and GSSG. TGR was first discovered in *S. mansoni* [53] and since then, it has been reported in a number of parasitic flukes, including *S. japonicum*, *F. hepatica*, and *F. gigantica* [16, 36, 58, 59]. TGR is also present in mammals, albeit in low amounts. It is expressed in male germ cells and found only at low levels in other tissues [54, 60]. Parasitic flukes lack catalase, and in the absence of catalase, the thiol redox homeostasis of these parasites depends completely on TGR. TGR is the main enzyme responsible for the maintenance of redox homeostasis, ROS detoxification, and deoxyribonucleotides synthesis in these organisms. Unlike GR, TrxR and TGR enzymes contain a C-terminal extension of 16 amino acids, where an additional active site (-GCUG-) is located and is indispensable for most functions of these enzymes. TGR is characterized as selenoenzymes, with Sec occurring as the penultimate amino acid in the redox center -GCUG-. Selenium has multifunctional importance in selenoenzymes. It is a homolog of Cys with the thiol chain replaced by selenol moiety. We propose that, Sec is more nucleophilic than sulfur, and

therefore, its presence may increase the reaction rate of Sec-containing enzymes. Though it has been shown that replacement of sulfur with selenium in a thiol/disulfide exchange reaction accelerates the rate of reaction whether selenium acts as a nucleophile, electrophile, or leaving group [61]. Additionally, after reacting with substrates, the resultant thiol-selenolate may efficiently accept electrons from other redox-active Cys pairs as Sec has a lower pKa value than Cys, making it a better leaving group. In addition, under the conditions of oxidative stress, selenoenzymes are more resistant to inactivation by irreversible oxidation than Cys-containing enzymes.

In the present study, we studied the catalytic and structural properties of different variants of *Fasciola gigantica* TGR to understand the role of Sec. The ORF of FgTGR was fused with a bacterial type SECIS element by PCR to form a chimeric gene. We constructed three enzyme forms- full-length Sec containing TGR (FgTGRsec), TGR without Sec and the last amino acid (FgTGR) and TGR without the N-terminal Grx domain ( $\Delta$ NTD-FgTGRsec). All the three proteins were purified, and the SEC results suggest that all three proteins exist as dimers in solution and that the TrxR domain is responsible for dimerization of the subunits. We further examined the structural properties of the proteins and found the proteins to be in a properly folded conformation. A lower value of fluorescence emission maxima for FgTGR relative to FgTGRsec implies slight compactness of the protein without a Sec tail end. The  $\Delta$ NTD-FgTGRsec shows comparatively higher fluorescence emission maxima relative to both FgTGRsec and FgTGR. This may be due to the absence of the Grx domain that leads to slight exposure of certain Trp residues towards solvent.

We observed that FgTGRsec shows higher DTNB-based TrxR and GR activity than FgTGR. This property of the enzyme may be attributed to the presence of the Sec. The C-terminal selenotetrapeptide of TGR is known to shuttle electrons from NADPH to both Trx and GSSG [11]. Also, at physiological pH, the selenol of Sec is mainly in its anionic (pKa 5.2) form. This lower pKa value and stronger nucleophilicity make FgTGRsec more reactive than FgTGR [11]. To study the role of the Grx domain in the DTNB-based TrxR activity of FgTGRsec, we performed comparative binding analysis of DTNB with FgTGRsec and  $\Delta$ NTD-FgTGRsec. The result suggests that the binding of DTNB was partly compromised in the  $\Delta$ NTD-FgTGRsec. The decrease in binding efficiency of DTNB towards  $\Delta$ NTD-FgTGRsec might be because of some structural perturbations that occurred due to the absence of the Grx domain. The comparative

activity assays also confirmed this observation. GR activity studies suggested that the Sec was required for the transfer of electrons from the thiol/disulfide active site of FgTGR to the Grx domain. Thus, the physiologically relevant NADPH dependent activities of FgTGR were dependent on Sec. These results suggest that the Sec is responsible for higher DTNB-based TrxR and GR activity in FgTGRsec and that the N-terminal Grx domain positively regulates DTNB-based TrxR activity. It was also observed that like other dithiolic Grx domain containing TGRs, the GR activity of FgTGRsec exhibited a hysteretic kinetic behavior at high GSSG concentrations (Supplementary Fig. 11).

The structure of FgTGRsec was modeled using the crystal structure of SjtGR as a template. The RMSD showed an excellent value of 0.277 Å indicating the accuracy of the structure. AF is a well-known inhibitor for TGR of parasitic flukes [7, 30]. It is a pro-drug that delivers the gold-containing compound to Sec containing flavoreductases (TrxR and TGR) more effectively than non-Sec containing ones (GR) where this preference has been attributed to the high affinity of selenium for gold [62]. Structurally, it has a linear two coordinated Au(I) center with a TP-gold ligand and a tetraacetylthioglucose ligand (Supplementary Figure 12). The phosphine moiety confers membrane solubility to AF, whereas the tetraacetylthioglucose ligand is excreted *in vivo*, suggesting that the TP-gold is the active therapeutic compound [63]. AF inhibits SmTGR at a nanomolar concentration ( $IC_{50} \sim 7$  nM) and subsequently reduces worm burden in mice [7, 56]. We observed that the disulfide reductase activity of FgTGRsec was inhibited by AF, suggesting that FgTGR is dependent on Sec with an  $IC_{50}$  of 0.87  $\mu$ M for DTNB-based TrxR activity and 8.3  $\mu$ M for GR activity. Molecular docking studies showed that the binding of AF can change the conformation of the enzyme and lead to stop the electron flow. His571 is a key catalytic residue in the formation of selenolate anion that is conserved in human and *Plasmodium* TrxR and other TGR homologs from parasitic flukes [14, 64, 65]. The gold can reach and interact with the His571 residue of FgTGRsec leading to the disruption of the electron transfer mechanism. Such interaction of gold and His residue of various selenoenzymes have been shown in previous studies [66, 67] and thus validate our observation.

Lastly, we compared the folding and conformational stabilities of Sec containing and non-containing TGR and also determined the role of the Grx domain in the folding and stability. The results were compared with the activity data. To our knowledge, no other investigation to date has been performed to study the unfolding and stability parameters of any TGR. Our results

indicate that GdnHCl induces cooperative unfolding of the proteins without stabilization of any intermediate state (Fig. 7A). The  $C_m$  of FgTGRsec was found to be lower than that of FgTGR suggesting that FgTGRsec is comparatively less stable than FgTGR. The  $C_m$  value represents the midpoint of unfolding transition, higher the  $C_m$ , more stable is the nature of the protein. A greater  $\Delta G_D^{H20}$  value for FgTGR than that of FgTGRsec further validates the more stable nature of FgTGR. The lesser stability of the full-length enzyme could be explained by the presence of Sec in the C-terminal that makes the protein flexible to be catalytically more active. This type of flexibility could be also a prerequisite for facilitating proper binding/positioning of the cofactors and substrates into their respective pockets, which also correlates with our activity results. The decrease in the fluorescence polarization as well as the GR and DTNB-based TrxR activity of FgTGRsec and FgTGR suggests perturbation in the binding of the co-factors to the enzyme. Our result suggests that slight variations in binding/orientation of the FAD may lead to complete loss of enzymatic activity of flavoproteins due to the release of protein-bound FAD molecule [66, 68]. The comparative unfolding of FgTGRsec and  $\Delta$ NTD-FgTGRsec showed that the  $C_m$  of  $\Delta$ NTD-FgTGRsec is less than FgTGRsec, indicating that it is reasonably less stable than FgTGRsec. This suggests that the presence of the Grx domain enhances the stability of the enzyme and may be attributed to increased favorable interactions between the domains. These results demonstrate the role of the Grx domain in maintaining the integrity of the FgTGRsec structure and that the absence of the Grx domain in the  $\Delta$ NTD-FgTGRsec makes the structure susceptible to denaturation at lower GdnHCl concentration.

## 5. CONCLUSIONS

TGR plays an indispensable role in the redox biochemistry of parasitic flukes. Several studies validated TGR as a novel drug target and identified potential leads that show great promise for treatment of parasitic helminth infections by disrupting redox homeostasis. We investigated the biochemical and structural properties of different variants of *F. gigantica* TGR to understand the role of Sec and the Grx domain. Our results showed that Sec597 is responsible for higher TrxR and GR activity of FgTGRsec and the N-terminal Grx domain positively regulates the TrxR activity of FgTGRsec. The unfolding experiments suggested that FgTGR without Sec was more stable in solution than FgTGRsec and  $\Delta$ NTD-FgTGRsec. The unique properties of TGR in *F. gigantica* make it a promising target for developing new treatments for fascioliasis.

**Acknowledgements**

The authors thank Dr. Rajanish Giri, IIT Mandi for help with CD experiments. PK thanks NEHU for providing Non-NET fellowship. RS and HS thank UGC, New Delhi, India for providing fellowships.

**Competing interest**

The authors declare that there are no competing interests.

**Author's contributions**

Conceived and designed the experiments: PK, RS, HS, TT.

Performed the experiments: PK, RS.

Analyzed the data: PK, RS, HS, TT.

Contributed reagents/materials/analysis tools: PK, RS, HS, TT.

Wrote the paper: PK, RS, HS, TT.

**Abbreviations**

Thioredoxin glutathione reductase, TGR; glutaredoxin, Grx; thioredoxin reductase, TrxR; glutathione reductase, GR; Sec containing TGR, FgTGRsec; TGR without Sec, FgTGR; TGRsec without the N-terminal Grx domain,  $\Delta$ NTD-FgTGRsec; auranofin, AF; selenocysteine, Sec; 5,5'-dithiobis(2-nitrobenzoic acid), DTNB; oxidized glutathione, GSSG; reduced glutathione, GSH; triethylphosphine-gold, TP gold; midpoint of unfolding transition,  $C_m$ ; free energy of stabilization in the absence of denaturants,  $\Delta G_D^{H_2O}$ .

**REFERENCES**

- [1] J. Nordberg, E.S. Arner, Reactive oxygen species, antioxidants, and the mammalian thioredoxin system, *Free Radic Biol Med*, 31 (2001) 1287-1312.
- [2] C. Berndt, C.H. Lillig, A. Holmgren, Thioredoxins and glutaredoxins as facilitators of protein folding, *Biochim Biophys Acta*, 1783 (2008) 641-650.
- [3] T. Tripathi, S. Suttiprapa, B. Sripra, Unusual thiol-based redox metabolism of parasitic flukes, *Parasitol Int*, 66 (2017) 390-395.

- [4] G. Salinas, M.E. Selkirk, C. Chalar, R.M. Maizels, C. Fernandez, Linked thioredoxin-glutathione systems in platyhelminths, *Trends Parasitol*, 20 (2004) 340-346.
- [5] M. Bonilla, S.M. Denicola A Fau - Marino, V.N. Marino Sm Fau - Gladyshev, G. Gladyshev Vn Fau - Salinas, G. Salinas, Linked thioredoxin-glutathione systems in platyhelminth parasites: alternative pathways for glutathione reduction and deglutathionylation, *J. Biol. Chem.*, 286(7) (2011) 4959-4967.
- [6] L. Otero, M. Bonilla, A.V. Protasio, C. Fernandez, V.N. Gladyshev, G. Salinas, Thioredoxin and glutathione systems differ in parasitic and free-living platyhelminths, *BMC Genomics*, 11 (2010) 237.
- [7] A.N. Kuntz, E. Davioud-Charvet, A.A. Sayed, L.L. Califf, J. Dessolin, E.S. Arner, D.L. Williams, Thioredoxin glutathione reductase from *Schistosoma mansoni*: an essential parasite enzyme and a key drug target, *PLoS Med*, 4 (2007) e206.
- [8] D.L. Williams, M. Bonilla, V.N. Gladyshev, G. Salinas, Thioredoxin glutathione reductase-dependent redox networks in platyhelminth parasites, *Antioxidants & redox signaling*, 19 (2013) 735-745.
- [9] G.M. Mkoji, J.M. Smith, R.K. Prichard, Antioxidant systems in *Schistosoma mansoni*: Evidence for their role in protection of the adult worms against oxidant killing, *International Journal for Parasitology*, 18 (1988) 667-673.
- [10] J. Lu, A. Holmgren, Selenoproteins, *J Biol Chem*, 284 (2009) 723-727.
- [11] D.L. Hatfield, M.J. Berry, V.N. Gladyshev, Selenium: its molecular biology and role in human health, Springer Science & Business Media, 2011.
- [12] Y. Li, Q. Wu, Y. Peng, F. Huang, X. Li, L. Chen, D. Shi, X. Zhou, X. Fan, Expression, crystallization and preliminary X-ray diffraction analysis of thioredoxin glutathione reductase from *Schistosoma japonicum* in complex with FAD, *Acta Crystallogr F Struct Biol Commun*, 70 (2014) 92-96.
- [13] J.L. Rendon, I.P. del Arenal, A. Guevara-Flores, A. Uribe, A. Plancarte, G. Mendoza-Hernandez, Purification, characterization and kinetic properties of the multifunctional thioredoxin-glutathione reductase from *Taenia crassiceps* metacestode (cysticerci), *Mol Biochem Parasitol*, 133 (2004) 61-69.

- [14] H.-H. Huang, L. Day, C.L. Cass, D.P. Ballou, C.H. Williams, D.L. Williams, Investigations on the Catalytic Mechanism of Thioredoxin Glutathione Reductase (TGR) from *Schistosoma mansoni*, *Biochemistry*, 50 (2011) 5870-5882.
- [15] F. Angelucci, D. Dimastrogiovanni, G. Boumis, M. Brunori, A.E. Miele, F. Saccoccia, A. Bellelli, Mapping the catalytic cycle of *Schistosoma mansoni* thioredoxin glutathione reductase by X-ray crystallography, *J Biol Chem*, 285 (2010) 32557-32567.
- [16] A. Guevara-Flores, J.P. Pardo, J.L. Rendon, Hysteresis in thioredoxin-glutathione reductase (TGR) from the adult stage of the liver fluke *Fasciola hepatica*, *Parasitol Int*, 60 (2011) 156-160.
- [17] M. Bonilla, A. Denicola, S.V. Novoselov, A.A. Turanov, A. Protasio, D. Izmendi, V.N. Gladyshev, G. Salinas, Platyhelminth mitochondrial and cytosolic redox homeostasis is controlled by a single thioredoxin glutathione reductase and dependent on selenium and glutathione, *J Biol Chem*, 283 (2008) 17898-17907.
- [18] C. Brandstaedter, K. Fritz-Wolf, S. Weder, M. Fischer, B. Hecker, S. Rahlfs, K. Becker, Kinetic characterization of wild-type and mutant human thioredoxin glutathione reductase defines its reaction and regulatory mechanisms, *The FEBS journal*, (2017).
- [19] WHO, WHO estimates of the global burden of foodborne diseases, in, 2015.
- [20] S. Mas-Coma, M.A. Valero, M.D. Bargues, Fascioliasis, *Adv Exp Med Biol*, 766 (2014) 77-114.
- [21] S. Mas-Coma, R. Angles, J.G. Esteban, M.D. Bargues, P. Buchon, M. Franken, W. Strauss, The Northern Bolivian Altiplano: a region highly endemic for human fascioliasis, *Trop Med Int Health*, 4 (1999) 454-467.
- [22] M. Parkinson, S.M. O'Neill, J.P. Dalton, Endemic human fasciolosis in the Bolivian Altiplano, *Epidemiol Infect*, 135 (2007) 669-674.
- [23] G.C. Coles, Anthelmintic activity of triclabendazole, *J Helminthol*, 60 (1986) 210-212.
- [24] G.B. Mitchell, L. Maris, M.A. Bonniwell, Triclabendazole-resistant liver fluke in Scottish sheep, *Vet Rec*, 143 (1998) 399.
- [25] G.P. Brennan, I. Fairweather, A. Trudgett, E. Hoey, McCoy, M. McConville, M. Meaney, M. Robinson, N. McFerran, L. Ryan, C. Lanusse, L. Mottier, L. Alvarez, H. Solana, G. Virkel, P.M. Brophy, Understanding triclabendazole resistance, *Exp Mol Pathol*, 82 (2007) 104-109.

- [26] Y.M. Brockwell, T.P. Elliott, G.R. Anderson, R. Stanton, T.W. Spithill, N.C. Sangster, Confirmation of *Fasciola hepatica* resistant to triclabendazole in naturally infected Australian beef and dairy cattle, *Int J Parasitol Drugs Drug Resist*, 4 (2013) 48-54.
- [27] D. Gordon, R. Zadoks, P. Skuce, N. Sargison, Confirmation of triclabendazole resistance in liver fluke in the UK, *Vet Rec*, 171 (2012) 159-160.
- [28] J.M. Kelley, T.P. Elliott, T. Beddoe, G. Anderson, P. Skuce, T.W. Spithill, Current Threat of Triclabendazole Resistance in *Fasciola hepatica*, *Trends Parasitol*, 32 (2016) 458-469.
- [29] L. Song, J. Li, S. Xie, C. Qian, J. Wang, W. Zhang, X. Yin, Z. Hua, C. Yu, Thioredoxin glutathione reductase as a novel drug target: evidence from *Schistosoma japonicum*, *PLoS One*, 7 (2012) e31456.
- [30] A. Caroli, S. Simeoni, R. Lepore, A. Tramontano, A. Via, Investigation of a potential mechanism for the inhibition of SmtGR by Auranofin and its implications for *Plasmodium falciparum* inhibition, *Biochem Biophys Res Commun*, 417 (2012) 576-581.
- [31] R. Shukla, H. Shukla, P. Kalita, T. Tripathi, Structural insights into natural compounds as inhibitors of *Fasciola gigantica* thioredoxin glutathione reductase, *J Cell Biochem*, (2017).
- [32] B.J. Neves, R.F. Dantas, M.R. Senger, C.C. Melo-Filho, W.C. Valente, A.C. de Almeida, J.M. Rezende-Neto, E.F. Lima, R. Paveley, N. Furnham, E. Muratov, L. Kametsky, A.E. Carpenter, R.C. Braga, F.P. Silva-Junior, C.H. Andrade, Discovery of New Anti-Schistosomal Hits by Integration of QSAR-Based Virtual Screening and High Content Screening, *J Med Chem*, 59 (2016) 7075-7088.
- [33] T. Li, P.D. Ziniel, P.Q. He, V.P. Kommer, G.J. Crowther, M. He, Q. Liu, W.C. Van Voorhis, D.L. Williams, M.W. Wang, High-throughput screening against thioredoxin glutathione reductase identifies novel inhibitors with potential therapeutic value for schistosomiasis, *Infect Dis Poverty*, 4 (2015) 40.
- [34] F. Ross, P. Hernandez, W. Porcal, G.V. Lopez, H. Cerecetto, M. Gonzalez, T. Basika, C. Carmona, M. Flo, G. Maggioli, M. Bonilla, V.N. Gladyshev, M. Boiani, G. Salinas, Identification of thioredoxin glutathione reductase inhibitors that kill cestode and trematode parasites, *PLoS One*, 7 (2012) e35033.
- [35] C.C. Melo-Filho, R.F. Dantas, R.C. Braga, B.J. Neves, M.R. Senger, W.C. Valente, J.M. Rezende-Neto, W.T. Chaves, E.N. Muratov, R.A. Paveley, N. Furnham, L. Kametsky, A.E.

Carpenter, F.P. Silva-Junior, C.H. Andrade, QSAR-Driven Discovery of Novel Chemical Scaffolds Active against *Schistosoma mansoni*, *J Chem Inf Model*, 56 (2016) 1357-1372.

[36] A. Gupta, M. Kesharwani, D. Velmurugan, T. Tripathi, *Fasciola gigantica* thioredoxin glutathione reductase: Biochemical properties and structural modeling, *Int J Biol Macromol*, 89 (2016) 152-160.

[37] C.N. Pace, Determination and analysis of urea and guanidine hydrochloride denaturation curves, *Methods Enzymol*, 131 (1986) 266-280.

[38] H. Shukla, R. Shukla, A. Sonkar, T. Pandey, T. Tripathi, Distant Phe345 mutation compromises the stability and activity of *Mycobacterium tuberculosis* isocitrate lyase by modulating its structural flexibility, *Sci Rep*, 7 (2017) 1058.

[39] T. Tripathi, S. Rahlfs, K. Becker, V. Bhakuni, Structural and stability characteristics of a monothiol glutaredoxin: glutaredoxin-like protein 1 from *Plasmodium falciparum*, *Biochim Biophys Acta*, 1784 (2008) 946-952.

[40] T. Tripathi, Calculation of thermodynamic parameters of protein unfolding using far-ultraviolet circular dichroism, *J Protein Proteomics*, 4 (2013) 85-91.

[41] T. Tripathi, A. Roseler, S. Rahlfs, K. Becker, V. Bhakuni, Conformational stability and energetics of *Plasmodium falciparum* glutaredoxin, *Biochimie*, 92 (2010) 284-291.

[42] A. Fiser, A. Sali, Modeller: generation and refinement of homology-based protein structure models, *Methods Enzymol*, 374 (2003) 461-491.

[43] E.F. Pettersen, T.D. Goddard, C.C. Huang, G.S. Couch, D.M. Greenblatt, E.C. Meng, T.E. Ferrin, UCSF Chimera--a visualization system for exploratory research and analysis, *J Comput Chem*, 25 (2004) 1605-1612.

[44] M. Wiederstein, M.J. Sippl, ProSA-web: interactive web service for the recognition of errors in three-dimensional structures of proteins, *Nucleic Acids Res*, 35 (2007) W407-410.

[45] R.A. Laskowski, MacArthur, M.W., Moss, D.S., and Thornton, J.M., PROCHECK: a program to check the stereochemical quality of protein structures., *Journal of applied crystallography* 26 (1993) 283-291.

[46] R. Luthy, J.U. Bowie, D. Eisenberg, Assessment of protein models with three-dimensional profiles, *Nature*, 356 (1992) 83-85.

[47] R. Shukla, P.B. Chetri, A. Sonkar, M.Y. Pakharukova, V.A. Mordvinov, T. Tripathi, Identification of novel natural inhibitors of *Opisthorchis felinus* cytochrome P450 using

structure-based screening and molecular dynamic simulation, *J Biomol Struct Dyn*, (2017) 1-103.

[48] R. Shukla, H. Shukla, P. Kalita, A. Sonkar, T. Pandey, D.B. Singh, A. Kumar, T. Tripathi, Identification of potential inhibitors of *Fasciola gigantica* thioredoxin1: computational screening, molecular dynamics simulation, and binding free energy studies, *J Biomol Struct Dyn*, (2017) 1-16.

[49] R. Thomsen, M.H. Christensen, MolDock: a new technique for high-accuracy molecular docking, *J Med Chem*, 49 (2006) 3315-3321.

[50] J.T. Vivian, P.R. Callis, Mechanisms of tryptophan fluorescence shifts in proteins, *Biophys J*, 80 (2001) 2093-2109.

[51] J.R. Lakowicz, Principles of Fluorescence Spectroscopy, Springer US, 1983.

[52] A. Agorio, C. Chalar, S. Cardozo, G. Salinas, Alternative mRNAs arising from trans-splicing code for mitochondrial and cytosolic variants of *Echinococcus granulosus* thioredoxin Glutathione reductase, *J Biol Chem*, 278 (2003) 12920-12928.

[53] H.M. Alger, D.L. Williams, The disulfide redox system of *Schistosoma mansoni* and the importance of a multifunctional enzyme, thioredoxin glutathione reductase, *Mol Biochem Parasitol*, 121 (2002) 129-139.

[54] D. Su, S.V. Novoselov, Q.A. Sun, M.E. Moustafa, Y. Zhou, R. Oko, D.L. Hatfield, V.N. Gladyshev, Mammalian selenoprotein thioredoxin-glutathione reductase. Roles in disulfide bond formation and sperm maturation, *J Biol Chem*, 280 (2005) 26491-26498.

[55] F. Angelucci, A.E. Miele, G. Boumis, D. Dimastrogiovanni, M. Brunori, A. Bellelli, Glutathione reductase and thioredoxin reductase at the crossroad: the structure of *Schistosoma mansoni* thioredoxin glutathione reductase, *Proteins*, 72 (2008) 936-945.

[56] F. Angelucci, A.A. Sayed, D.L. Williams, G. Boumis, M. Brunori, D. Dimastrogiovanni, A.E. Miele, F. Pauly, A. Bellelli, Inhibition of *Schistosoma mansoni* thioredoxin-glutathione reductase by auranofin: structural and kinetic aspects, *J Biol Chem*, 284 (2009) 28977-28985.

[57] G. Salinas, W. Gao, Y. Wang, M. Bonilla, L. Yu, A. Novikov, V.G. Virginio, H.B. Ferreira, M. Vieites, V.N. Gladyshev, D. Gambino, S. Dai, The Enzymatic and Structural Basis for Inhibition of *Echinococcus granulosus* Thioredoxin Glutathione Reductase by Gold(I), *Antioxidants & redox signaling*, 27 (2017) 1491-1504.

- [58] L.J. Song, C.X. Yu, S.Y. Xie, X.R. Yin, C.Y. Qian, J. Wang, W. Zhang, X.D. Ke, Expression and characterization of thioredoxin glutathione reductase of *Schistosoma japonicum*, *Zhongguo Xue Xi Chong Bing Fang Zhi Za Zhi*, 23 (2011) 412-418.
- [59] N. Changklungmoa, P. Kueakhai, K. Sangpairoj, P. Chaichanasak, W. Jaikua, S. Riengrojpitak, P. Sobhon, K. Chaithirayanon, Molecular cloning and characterization of *Fasciola gigantica* thioredoxin-glutathione reductase, *Parasitol Res*, 114 (2015) 2119-2127.
- [60] M.V. Gerashchenko, D. Su, V.N. Gladyshev, CUG start codon generates thioredoxin/glutathione reductase isoforms in mouse testes, *J Biol Chem*, 285 (2010) 4595-4602.
- [61] D. Steinmann, T. Nauser, W.H. Koppenol, Selenium and sulfur in exchange reactions: a comparative study, *The Journal of organic chemistry*, 75 (2010) 6696-6699.
- [62] K.P. Bhabak, B.J. Bhuyan, G. Mugesh, Bioinorganic and medicinal chemistry: aspects of gold (I)-protein complexes, *Dalton Transactions*, 40 (2011) 2099-2111.
- [63] S.S. Gunatilleke, C.A. de Oliveira, J.A. McCammon, A.M. Barrios, Inhibition of cathepsin B by Au(I) complexes: a kinetic and computational study, *J Biol Inorg Chem*, 13 (2008) 555-561.
- [64] T.W. Gilberger, R.D. Walter, S. Muller, Identification and characterization of the functional amino acids at the active site of the large thioredoxin reductase from *Plasmodium falciparum*, *J Biol Chem*, 272 (1997) 29584-29589.
- [65] W. Brandt, L.A. Wessjohann, The functional role of selenocysteine (Sec) in the catalysis mechanism of large thioredoxin reductases: proposition of a swapping catalytic triad including a Sec-His-Glu state, *Chembiochem*, 6 (2005) 386-394.
- [66] A. De la Rosa Miguel, J. Márquez Antonio, M. Vega José, Dissociation of FAD from the NAD(P)H-Nitrate Reductase Complex from *Ankistrodesmus braunii* and Role of Flavin in Catalysis, *Zeitschrift für Naturforschung C*, 37 (2014) 24-30.
- [67] J. Zou, P. Taylor, J. Dornan, S.P. Robinson, M.D. Walkinshaw, P.J. Sadler, First Crystal Structure of a Medicinally Relevant Gold Protein Complex: Unexpected Binding of, *Angew Chem Int Ed Engl*, 39 (2000) 2931-2934.
- [68] H.Y. Neujahr, Effect of anions, chaotropes, and phenol on the attachment of flavin adenine dinucleotide to phenol hydroxylase, *Biochemistry*, 22 (1983) 580-584.

## Figure Legends

**Figure 1. Purification of the recombinant proteins over Ni-NTA agarose.** (A) SDS-PAGE analysis of the purified proteins. Lanes 1–4 represent molecular weight markers, purified FgTGRsec, FgTGR and  $\Delta$ NTD-FgTGRsec, respectively. (B) SEC profile of native FgTGRsec, FgTGR and  $\Delta$ NTD-FgTGRsec. Molecular weight and oligomeric status of the recombinant proteins were determined on Superdex™ 200 10/300 GL column at pH 8.0 and 25 °C. The column was calibrated with standard molecular weight markers: Aldolase (158kDa), conalbumin (75 kDa), ovalbumin (44kDa) and ribonuclease A (13.7 kDa).

**Figure 2. Structural features of recombinant proteins.** (A) Tryptophan emission fluorescence spectra. (B) Far-UV CD spectra. In these figures, the black, red and green lines represent the data for FgTGRsec, FgTGR and  $\Delta$ NTD-FgTGRsec samples, respectively.

**Figure 3. Comparison of binding affinity of DTNB and GSSG with FgTGRsec and FgTGR using fluorescence quenching and activity assays.** (A) Stern–Volmer plot for the fluorescence intensity ( $F_0/F_1$ ) of FgTGRsec and FgTGR upon DTNB binding. (B) Comparative TrxR activity of FgTGRsec and FgTGR with DTNB. (C) Stern–Volmer plot for the fluorescence intensity ( $F_0/F_1$ ) of FgTGRsec and FgTGR upon GSSG binding. (D) Comparative GR activity of FgTGRsec and FgTGR with GSSG. In these figures the solid squares with solid line represents FgTGRsec and the hollow squares with dotted line represents FgTGR, respectively.

**Figure 4. Comparison of DTNB binding affinity to FgTGRsec and  $\Delta$ NTD-FgTGRsec with fluorescence quenching and activity assays.** (A) Stern–Volmer plot for the fluorescence intensity ( $F_0/F_1$ ) of  $\Delta$ NTD-FgTGRsec upon DTNB binding. (B) Comparative TrxR activity of FgTGRsec and  $\Delta$ NTD-FgTGRsec with DTNB. In these figures the solid squares with solid line represents FgTGRsec and the hollow circles with dotted line represents  $\Delta$ NTD-FgTGRsec, respectively.

**Figure 5. Inhibition of FgTGRsec by AF.** (A) Stern–Volmer plot for the fluorescence intensity ( $F_0/F_1$ ) of FgTGRsec upon AF binding, where the solid squares represents FgTGRsec (B)

Inhibition of TrxR activity and GR activity of FgTGRsec by AF. (C) Calculation of  $IC_{50}$  by plotting percent inhibition of activity against log of [AF]. In figures (B) and (C) The solid squares represents Trx activity and hollow squares represents GR activity of FgTGRsec, respectively.

**Figure 6. The potential binding poses for the Auranofin and TP-gold moiety.** (A) Auranofin, and, (B) TP-gold moiety. The sphere represents the gold atom. Red dotted lines represent the hydrogen bonds.

**Figure 7. Comparison of GdnHCl induced unfolding of FgTGRsec and FgTGR.** (A) Effect of increasing GdnHCl concentrations on the CD ellipticity at 222 nm and the tryptophan emission wavelength maxima of FgTGRsec and FgTGR. The data is presented as fraction unfolded with the value observed in absence of GdnHCl taken as 0%. (B) Calculation of free energy,  $\Delta G_D^{H_2O}$  of unfolding in absence of denaturants from both CD and fluorescence signals. In figures (A) and (B) the solid squares, solid circles represent data for fluorescence and CD of FgTGRsec and; the hollow squares and hollow circles represent data for FgTGR, respectively. (C) and (D) Effect of GdnHCl on activity and polarization of FAD. The solid circles (black) and solid circles (red) represent activity of FgTGRsec and FgTGR respectively. The solid triangles (black) and solid triangles (red) represent change in FAD polarization of FgTGRsec and FgTGR, respectively.

**Figure 8. Comparison of GdnHCl induced unfolding of FgTGRsec and  $\Delta$ NTD-FgTGRsec.** (A) Effect of increasing GdnHCl concentrations on the CD ellipticity at 222 nm and the tryptophan emission wavelength maxima of FgTGRsec and  $\Delta$ NTD-FgTGRsec. The data is presented as fraction unfolded with the value observed in absence of GdnHCl taken as 0 %. In figures (A) and (B) the solid squares, solid circles represent data for fluorescence and CD of FgTGRsec and; the hollow squares and hollow circles represent data for  $\Delta$ NTD-FgTGRsec, respectively. (B) Calculation of free energy,  $\Delta G^{H_2O}$  of unfolding in absence of denaturants from both CD and fluorescence signals. (C) Effect of GdnHCl on TrxR activity and polarization of FAD. The solid circles (black) and solid circles (red) represent TrxR activity of FgTGRsec and

$\Delta$ NTD-FgTGRsec respectively. The solid triangles (black) and solid triangles (red) represent change in FAD polarization of FgTGRsec and  $\Delta$ NTD-FgTGRsec, respectively.

ACCEPTED MANUSCRIPT

**Table 1. Stern Volmer quenching constants ( $K_{SV}$ ) in  $\mu\text{M}^{-1}$ .**

<b>Quencher</b>	<b>FgTGRsec</b>	<b>FgTGR</b>	<b><math>\Delta\text{NTD-FgTGRsec}</math></b>
<b>DTNB</b>	$60.6 \times 10^{-3}$	$42.5 \times 10^{-3}$	$52.2 \times 10^{-3}$
<b>GSSG</b>	$0.7 \times 10^{-3}$	$0.5 \times 10^{-3}$	ND
<b>Auranofin</b>	$58.8 \times 10^{-3}$	-	-

**Table 2. Thermodynamic parameters for GdnHCl-induced unfolding of FgTGRsec, FgTGR and  $\Delta$ NTD-FgTGRsec.**

Enzyme	Parameters	$\Delta G_D^{H_2O}$ (kcal.mol <sup>-1</sup> )	Average $\Delta G_D^{H_2O}$ (kcal.mol <sup>-1</sup> )	Average $C_m$ [M]
<b>FgTGRsec</b>	Far-UV CD	16.24	16.28	~2.1
	Trp fluorescence	16.32		
<b>FgTGR</b>	Far-UV CD	17.35	17.66	~2.4
	Trp fluorescence	17.96		
<b><math>\Delta</math>NTD-FgTGRsec</b>	Far-UV CD	15.91	15.94	~1.9
	Trp fluorescence	15.98		

**Highlights**

- We investigated the catalytic and thermodynamic properties of different variants of FgTGR to understand the role of Sec.
- Biochemical studies revealed that Sec597 is responsible for TrxR and GR activity of FgTGRsec.
- The N-terminal Grx domain positively regulates the TrxR activity of FgTGRsec.
- Unfolding studies suggest that all three proteins are highly cooperative molecules.
- FgTGR without Sec was more stable in solution than the other protein variants.
- To our knowledge, this is the first report on unfolding and stability analysis of any TGR.

ACCEPTED MANUSCRIPT

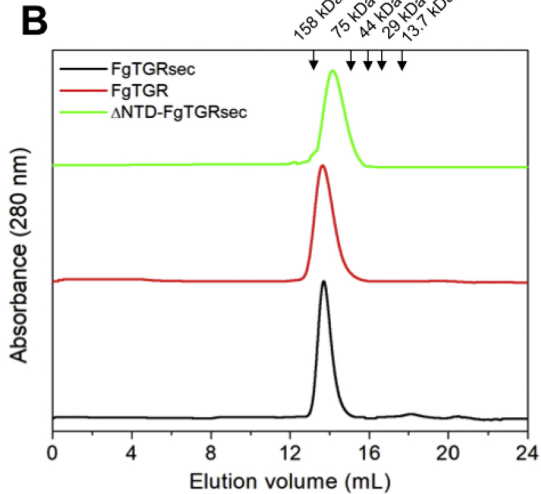
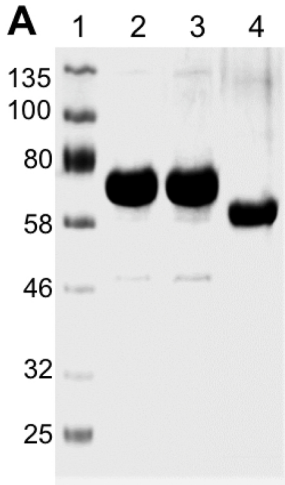


Figure 1

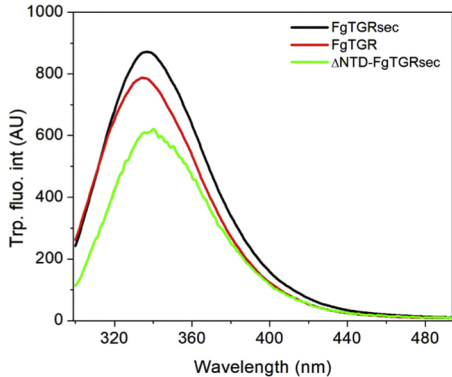
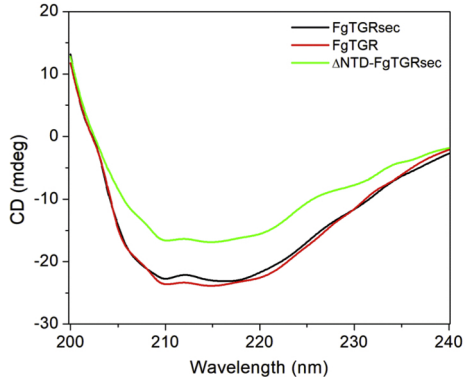
**A****B**

Figure 2

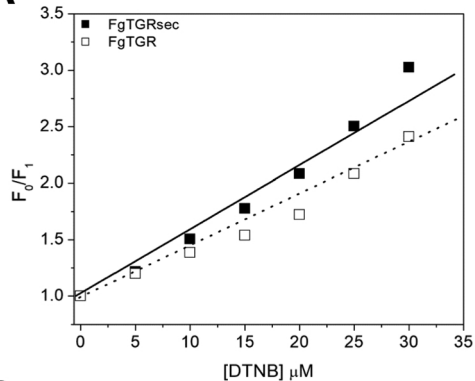
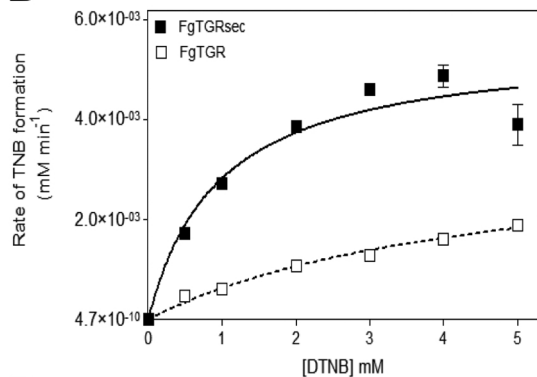
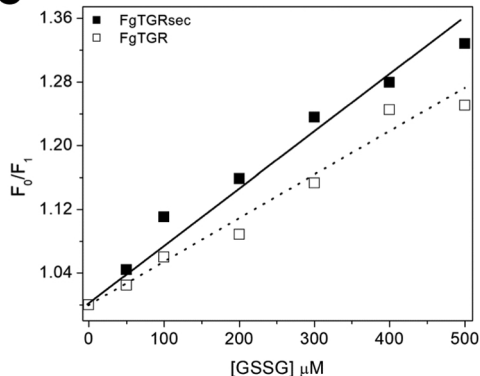
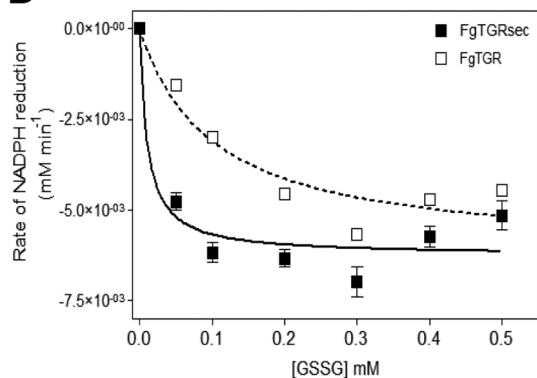
**A****B****C****D**

Figure 3

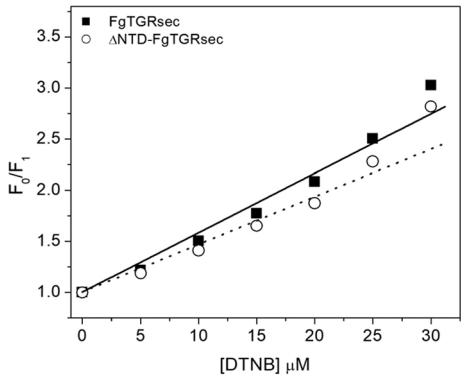
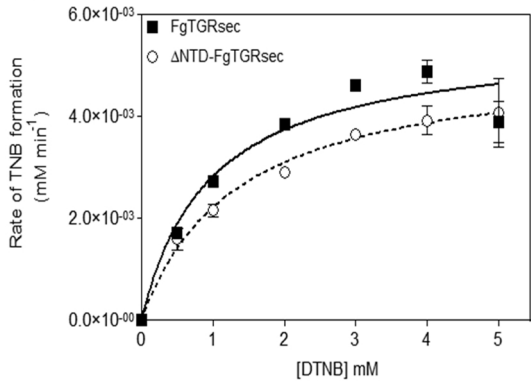
**A****B**

Figure 4

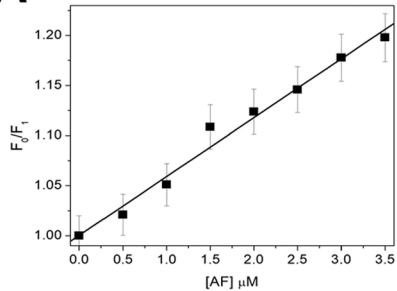
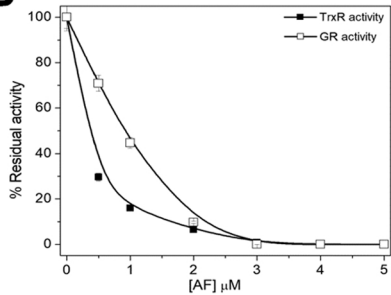
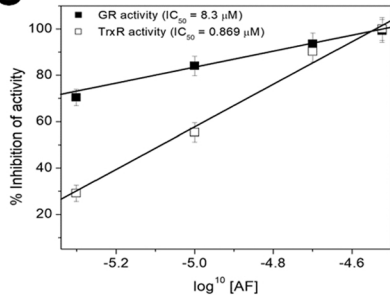
**A****B****C**

Figure 5

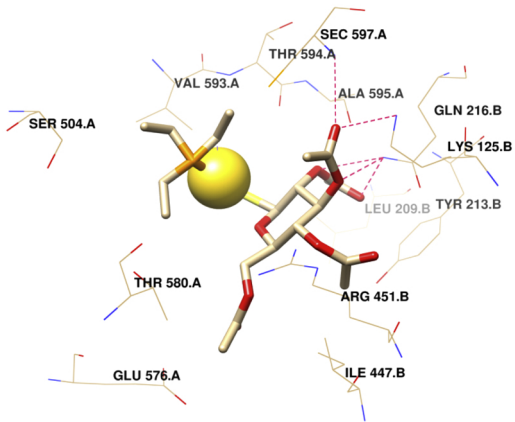
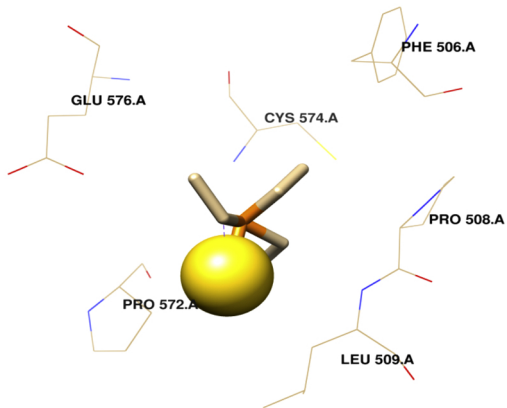
**A****B**

Figure 6

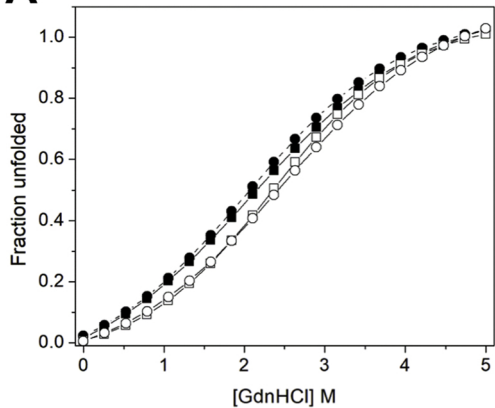
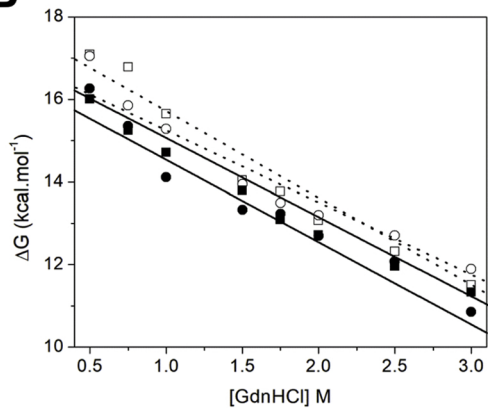
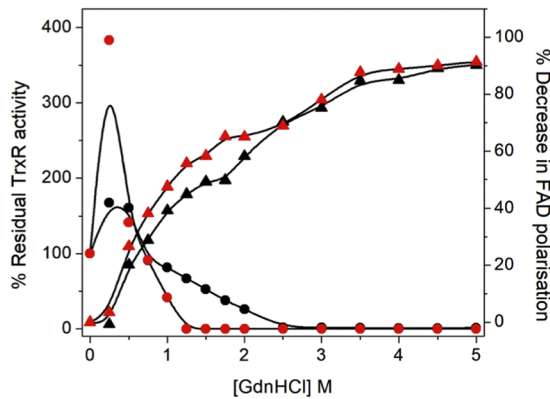
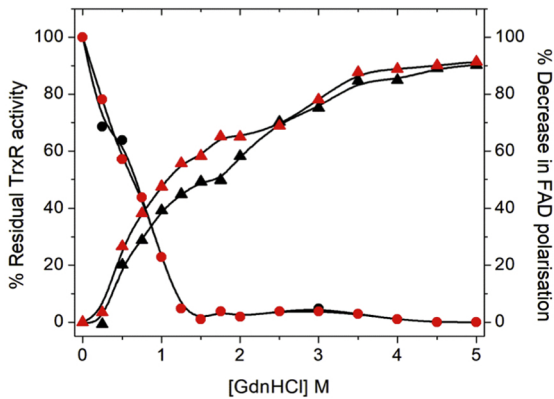
**A****B****C****D**

Figure 7

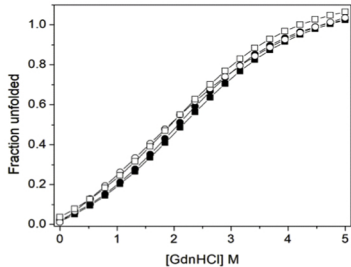
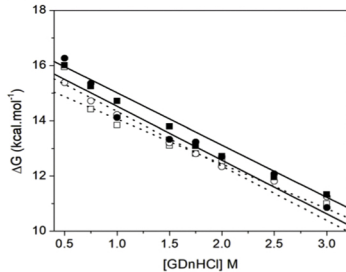
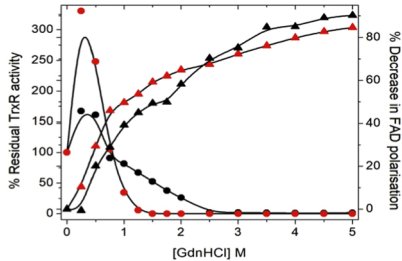
**A****B****C**

Figure 8